ACS APPLIED NANO MATERIALS
Cite This: ACS Appl. Nano Mater. 2019, 2, 1857−1865
Article
www.acsanm.org

Synthesis of Scintillating Ce^{3+}-Doped $Lu_2Si_2O_7$ Nanoparticles Using the Salt-Supported High Temperature (SSHT) Method: Solid State Chemistry at the Nanoscale

Shani Egodawatte,[†] Eric Zhang,[‡] Tessa J. Posey,[†] Grayson R. Gimblet,[†] Stephen H. Foulger,[‡] and Hans-Conrad zur Loye*,[†]

[†]Department of Chemistry and Biochemistry, University of South Carolina, Columbia, South Carolina 29208, United States
[‡]Department of Materials Science and Engineering, Clemson University, Clemson, South Carolina 29634, United States

Supporting Information

ABSTRACT: The synthesis of lutetium silicate nanoparticles doped with Ce^{3+} using the new salt-supported high temperature (SSHT) method is reported. This mechanochemical−thermal method enables the synthesis of nanoparticles without aggregation even after long calcination times of 48 h at high temperatures. These nanoparticles are characterized by powder X-ray diffraction (PXRD), transmission electron microscopy (TEM), energy dispersive spectroscopy (EDS), and Fourier transform infrared spectroscopy (FT-IR). Their optical properties, including UV luminescence and X-ray scintillation, are reported. These nanoparticles show strong luminescent and scintillation behavior. This SSHT method is general and can be used for the synthesis of other ternary and quaternary nanoparticle systems.

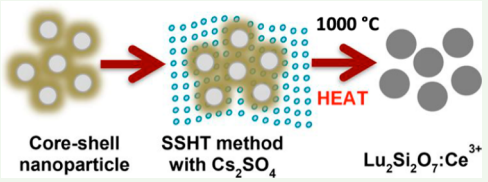

KEYWORDS: *core−shell, scintillation, radioluminescence, salt supported high temperature, dispersed nanoparticles, lutetium pyrosilicate*

INTRODUCTION

The formation of simple binary nanoparticles such as SiO_2, Al_2O_3, and Fe_3O_4 has essentially become a routine process, as many groups have developed numerous approaches for their synthesis.[1−5] This is not to say that for each system different synthetic variables do not still have to be optimized, but in general it is understood how one can obtain simple systems, such as CdTe, on the nanoscale with a desired nanoparticle size.[6,7] The situation becomes more complicated if one targets the synthesis of ternary nanoparticles; however, even here, many examples exist in the literature where in a single step ternary nanoparticles can be synthesized and their size controlled.[8,9] The synthesis of crystallographically ordered quaternary nanoparticles, however, remains a significant challenge due to the difficultly of combining multiple elements, achieving chemical reactivity between the elements, and still maintaining a product particle size at the nanoscale.

Simultaneous with optimizing nanoparticle synthesis, numerous approaches for manipulating nanoparticles via postsynthetic modification were developed, such as creating a core−shell structure, which has become a general, widely used, and highly successful process.[10,11] In this paper we are presenting our synthetic strategy to create quaternary nanoparticles, herein termed the "salt-supported high temperature (SSHT) method", by combining a variety of proven approaches, including solution precipitation and formation of core−shell structures, but adding an important new step that enables us to create complex oxide structures by performing high temperature solid state reactions at the nanoscale while maintaining the nanosize of our product material. The basic premise of the SSHT approach is to disperse preprepared core−shell structures on salt powders, such as Cs_2SO_4 powders, thereby spatially isolating the core−shell nanoparticles sufficiently from each other so that they can be heated to high temperatures (1000 °C) without leading to particle aggregating and loss of their nanosize.[12] Via this approach, we have succeeded in preparing 100 nm scintillating Ce^{3+}-doped $Lu_2Si_2O_7$ nanoparticles, $Lu_2Si_2O_7:Ce^{3+}$.

Scintillators—materials that can both absorb high energy radiation and convert this energy into excited states in active luminescence centers for light emission—have many uses ranging from X-ray phosphors to PET and CT scanners, X-ray and neutron detectors, homeland security for improved nuclear detection systems, and other diverse medical applications.[13−16] Among scintillators, the lanthanide pyrosilicate compounds ($Ln_2Si_2O_7$) (Ln = lanthanide) doped with active lanthanide ions (Ce^{3+}, Tb^{3+}, and Eu^{3+}) are among some of the most promising scintillators known.[17,18] $Lu_2Si_2O_7:Ce^{3+}$ is a promising scintillator material which has high light outputs without afterglow, fast scintillation decay times, and stable light outputs at high temperature.[19−21] In comparison to most other scintillating materials, such as lanthanide orthosilicates, $LnSiO_5$, and lanthanide aluminates, such as $Ln_3Al_5O_{12}$ and $LnAlO_3$, the pyrosilicates display lower crystallization temper-

Received: November 26, 2018
Accepted: March 20, 2019
Published: March 20, 2019

DOI: 10.1021/acsanm.8b02146
ACS Appl. Nano Mater. 2019, 2, 1857−1865

atures and good thermal stability.[22−24] Among all of the pyrosilicate phases known, $Y_2Si_2O_7$ and $Lu_2Si_2O_7$ have been the most studied phases due to their high light output under X-ray irradiation, while $Gd_2Si_2O_7$:Ce^{3+} is of interest due to its short decay time and low afterglow level.[25−27] By comparison, $La_2Si_2O_7$:Ce^{3+} is used significantly less frequently as a host matrix due to synthetic challenges.[28,29] Recently, its photoluminescence properties were explored by doping it with Ce^{3+}, Tb^{3+}, and Eu^{3+}, which resulted in strong X-ray luminescence, a fast decay time, and good thermal stability.[30,31]

These pyrosilicate compounds have been synthesized using a variety of methods, including single crystal growth, sol−gel, hydrothermal, solid state, and ceramic methods as well as nanocrystallization methods for glass.[17,32−36] The major drawback of most of these procedures is the long time required for calcination, and in addition, this long calcination time results in large, aggregated, sintered particles.[37] The field of nanoscience focuses on the synthesis of nanoparticles for applications where either large particles cannot be used or where the desired properties, often optical, are specific to the nanosize of the particle and different from the bulk.[38] This has led to the use of nanomaterials for medical applications where large particles cannot be used.[39−41] These nanoparticles are specifically designed for the use of optogenetic studies.

Herein we describe the development of a method for the preparation of Ce^{3+}-doped $Lu_2Si_2O_7$ nanoparticles using a facile core−shell method, which gives substantial control over size and the morphology of the nanoparticles, followed by the SSHT method to create fully reacted crystalline nanoparticles. The paper focuses on this methodology, the effect of annealing temperature on the crystallinity of these nanoparticles, and the effect of the dopant concentration (Ce^{3+}) on the luminescence and the scintillating properties.

RESULTS AND DISCUSSION

The ability to create complex nanoparticles relies on our ability to (1) create nanosized precursor particles, (2) react these particles under conditions where the constituent elements can react and form the product phase, and (3) avoid sintering of the nanoparticles. To achieve this, we combined the core−shell approach with the "salt-supported high temperature" (SSHT) method to enable the formation of complex quaternary oxide structures by performing high temperature solid state reactions at the nanoscale while maintaining the nanosize of our product material.[12] Sintering was avoided by dispersing the preprepared core−shell structures on Cs_2SO_4 powders, thereby spatially separating the core−shell nanoparticles sufficiently to avoid sintering and aggregation while they were heated for extended times at 1000 °C. This combined approach enabled us to obtain 100 nm sized scintillating Ce^{3+}-doped $Lu_2Si_2O_7$ nanoparticles.

The core−shell method is a powerful approach to tailor the properties of nanoparticles by coating one nanoparticle with an outer shell consisting of a different chemical composition. The assembly of this core−shell architecture can be performed using very mild conditions, thereby exerting control over the core−shell particle size and morphology.[10,42] Depending on the composition, very little to very much heat is needed to react these core and shell compositions to give rise to one single phase. If only little heat is required, sintering of the nanoparticles is minimal and the spherical nanoparticle morphology can be retained. If, however, significant heat is required, typically sintering and aggregation take place. This is the case for lanthanide silicates, where the reaction between the SiO_2 core and the lanthanide coating requires substantial thermal energy.

The SiO_2 core consists of so-called Stober particles. In the synthesis of the Stober silica nanoparticles, the basic medium provided by the ammonium hydroxide hydrolyzes the TEOS, which is the silicon source. There are multiple factors that control the particle size, including the reaction temperature, time, and reagent concentration. When the temperature of the reaction is high, the amount of nucleation is high, which gives rise to many smaller particles. After an initial burst of nucleation that creates the "nucleus", the reaction is aged for 2 h to allow the monomers from the hydrolyzed silicon source to react with the surface of the existing "nucleus" and grow these particles. The mixture of water and methanol utilized as the solvent system slows down the hydrolysis of TEOS, which enables a tight control over the particle size.[43] By adjustment of the temperature, aging time, solvent system, and the amount of TEOS in the reaction mixture, sub-100 nm particles are created. A schematic representation of the synthesis of nanoparticles is given in Figure 1.

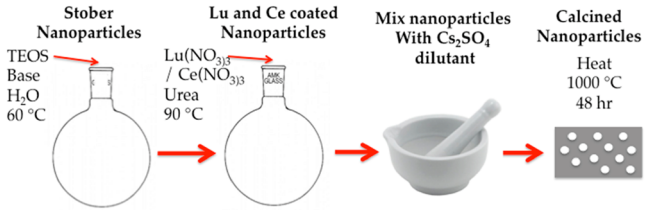

Figure 1. Schematic representation of the experimental procedure.

The Stober particles are coated with cerium and lutetium in a second step to create the core−shell structure. The silica samples are sonicated to ensure that the nanoparticles are homogeneously dispersed in the solution. This step is essential to form a homogeneous thin coating in the samples. NH_4OH provides the basic medium in this system, which gives the necessary pH under which the metal nitrates precipitate onto the surface of the nanoparticles.[42] As the solution conditions are very dilute, this gives rise to a very thin shell coating of the lanthanides on the silica nanoparticle surface. As shown in the TEM images of the as coated particles before calcination, very small aggregates can be seen on the surface of the nanoparticles as opposed to the original smoothness of the Stober nanoparticles (Figure 2B). To obtain individual nanoparticles that are not aggregated, the metal nitrate concentrations and the silica nanoparticle concentration were varied, and the optimum concentrations were determined as listed in Table 1.

The cerium concentration was adjusted to the optimum concentration at which these nanoparticles scintillated but remained as individual particles. We observed that with increasing cerium concentration the particles began to aggregate, and therefore the minimum concentration of cerium, to create scintillating nonaggregated nanoparticles, was used. It is important to point out that in all cases a final heating step is required to create the scintillating product phase. The core−shell structure neither lumineses nor scintillates as the structure and composition of the scintillating Ce^{3+}-doped $Lu_2Si_2O_7$ nanoparticles needs to be created first. Initial experiments focused on using very high temperatures, 1200 °C, for very short times, 15 min, to complete the reaction while avoiding sintering. Two complications with this approach

DOI: 10.1021/acsanm.8b02146
ACS Appl. Nano Mater. 2019, 2, 1857−1865

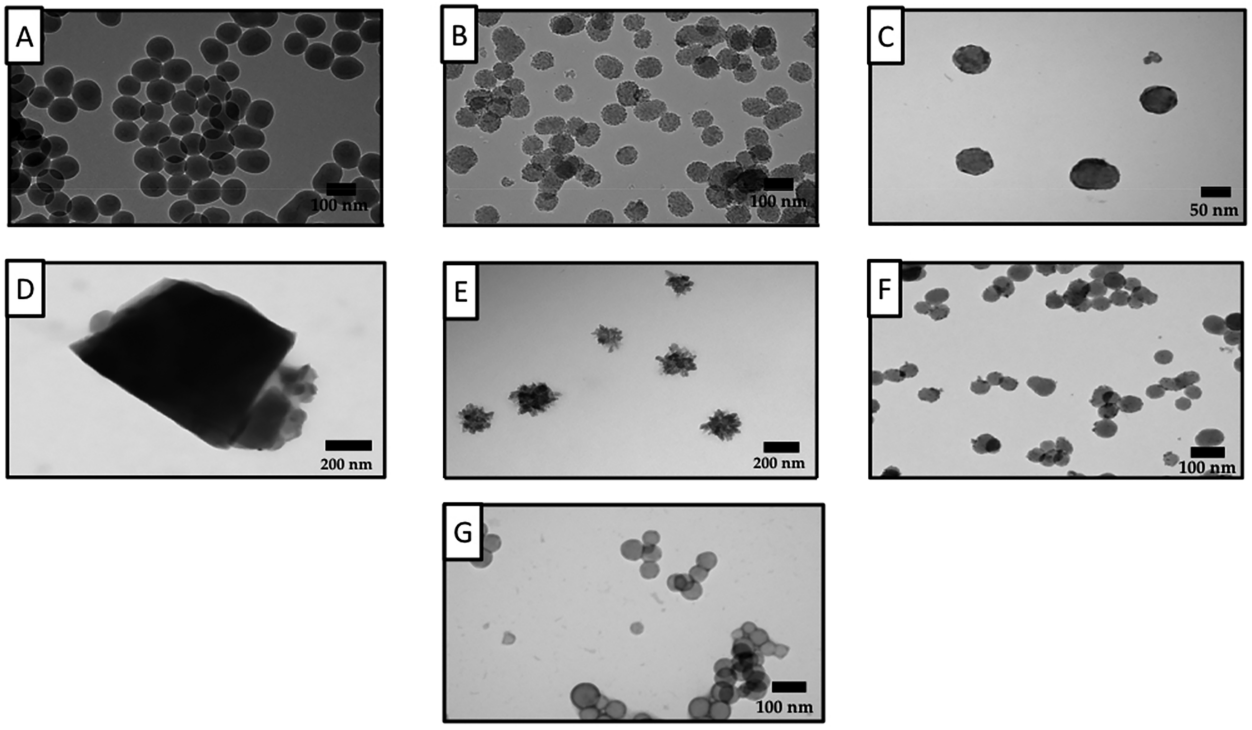

Figure 2. (A) TEM image of Stober nanoparticles. (B) TEM image of nanoparticles sequentially coated with lutetium and cerium. (C) TEM image of $Lu_2Si_2O_7$:Ce^{3+} nanoparticles calcined at 1000 °C with Cs_2SO_4 as the salt support. (D) TEM image of $Lu_2Si_2O_7$:Ce^{3+} nanoparticles calcined at 1000 °C with Cs_2SO_4 as the salt support and washed with 1 M HCl showing a change in the spherical morphology. (E) TEM image of $Lu_2Si_2O_7$:Ce^{3+} nanoparticles calcined at 1000 °C with Cs_2SO_4 as the salt support and washed with saturated NaCl showing etching of the nanoparticles. (F) TEM image of $Lu_2Si_2O_7$:Ce^{3+} nanoparticles calcined at 1000 °C with Cs_2SO_4 as the salt support and washed with 1 M NaCl. (G) TEM image of lutetium silicate:Ce^{3+} nanoparticles calcined at 1200 °C illustrating the aggregation of particles.

Table 1. Synthesis Conditions for the Experimental Procedure

sample	nanoparticle (np) concn (mg/mL)	$Ce(NO_3)_3$ or $Lu(NO_3)_3$ (g)	urea (g)	water (mL)
Ce-coated Stober silica	Stober np: 1	$Ce(NO_3)_3$: 0.10	0.746	50
Lu-coated Stober silica	Ce-coated np: 3.33	$Lu(NO_3)_3$: 0.4	0.337	15

were observed. Heating these particles in air results in the oxidation of Ce(III) to Ce(IV) (formation of CeO_2) and adjacent particles tend to neck together (Figure 2G). The first was avoided by heating the samples in a vacuum, while the second persisted. Nonetheless, the calcination process resulted in the successful reaction between the silica core and the rare earth shells of the particle react to form the orthosilicate phase. Figure 3 shows the relationship between luminescence, scintillation, and calcination time as a function of the amount of cerium incorporated into the nanoparticles when the precipitation of Lu and Ce onto the Stober silica nanoparticles was done in a single step. $Lu_2Si_2O_7$ was used for this study to establish the optimum doping concentration.

It was observed that sequential coating gave the best results not only in terms of dispersed nanoparticles but also in terms of their scintillating ability as the amount of dopant (cerium) on these nanoparticles could be controlled in this way. The particles needed to be coated first with the cerium and then with lutetium. If the nanoparticles were coated first with lutetium and then cerium, it was found that the lutetium shell redissolved and was replaced with cerium. If, on the other hand, the nanoparticles were coated first with cerium and then

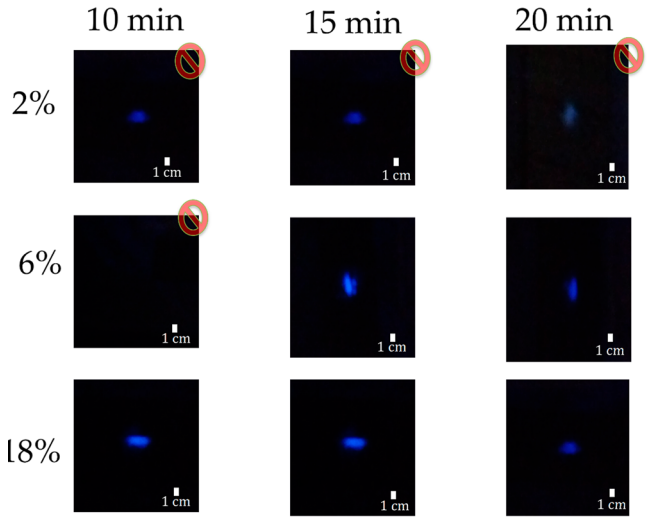

Figure 3. Optical images of the nanoparticles under UV irradiation. The luminescence intensity changes as a function of the amount of Ce^{3+} added. The rows indicate the amount of Ce^{3+} added in the coating procedure when utilizing a coprecipitation method. The columns indicate the optimum calcination time. Samples with a red mark did not scintillate under X-ray irradiation (Cu Kα, wavelength 1.5405 Å).

with lutetium, based on EDS measurements, the lutetium deposited on top of the cerium shell.

The amount of cerium added to the solution to prepare the core−shell structure was also found to be an important factor in the scintillating property of the fully reacted nanoparticles.

DOI: 10.1021/acsanm.8b02146
ACS Appl. Nano Mater. 2019, 2, 1857−1865

Figure 3 shows how the scintillation and luminescence properties change with the amount of cerium incorporated in the system. When the cerium content is low around 2% in the solution, the particles luminesced at longer calcination times but did not scintillate. When the amount of cerium was increased to 6% in the solution at longer calcination times, the samples luminesced and scintillated. At even higher cerium content at 18% the samples luminesced and scintillated. But it was not the ideal cerium concentration, as the increased cerium concentration gave rise to aggregation of particles. Further experiments were conducted with a concentration of 6% cerium. When the coprecipitation method was used, where cerium and lutetium were precipitated onto the silica nanoparticles in a single step, the addition of 6 wt % cerium with respect to lutetium concentration in the solution resulted in an ∼3% incorporation of cerium into the final product which, according to reports in the literature, is the optimum dopant concentration.[44,45] When the amount of cerium incorporated into the system was too low or too high, scintillating behavior was not observed. When a sequential coating procedure was used, the amount of Ce added in the first step was increased to 20 wt % with respect to Stober nanoparticles to obtain ∼3% incorporation in the final structure. When calcined in air, these nanoparticles also formed the CeO_2 phase, which leads to a decrease in available cerium for incorporation into the host orthosilicate structure, resulting in a decrease in the luminescing and scintillating ability of the nanoparticles. To avoid the formation of the CeO_2 phase, the unreacted, coated core−shell nanoparticles were sealed inside an evacuated silica tube during heating. This avoided the oxidation of Ce^{3+} to Ce^{4+}, thus increasing the scintillating ability of the particles for a given cerium concentration. EDS was used to obtain the approximate elemental composition of the nanoparticles which, after heating in vacuum and washing, were found to be Lu ∼ 15%, Ce ∼ 3%, Si ∼ 17%, and O ∼ 62%. The EDS spectrum and the data are shown in Figure S2 and Table S1, respectively.

The calcination temperature was also varied to understand how this affected aggregation and phase formation. The calcination temperature was varied from 800 to 1200 °C, where 1200 °C was found to be the temperature at which the nanoparticles completely reacted to form the desired phase in only 15 min. This process, however, gave rise to some aggregation. To avoid particle aggregation, the use of a water-soluble salt support was explored. The goal was to identify a salt support that is water-soluble and stable at high temperatures. One material that meets these criteria is Cs_2SO_4, which has a melting point of 1010 °C. Utilizing Cs_2SO_4 as the salt support at 1000 °C was found to be the optimum temperature at which the particles remained as individual particles, sintering was not observed, and the desired cerium doped lutetium silicate phase was obtained. Complete conversion to the target phase required calcination times of 48 h.

The particle size of the calcined nanoparticles was obtained from the powder X-ray diffraction patterns (Figure 4) using the Scherrer equation. The instrumental broadening was determined using the NIST LaB_6 standard and was used to obtain an accurate crystallite size using crystal diffraction (Figure S3). Based on peak broadening, the calcined nanoparticle had an average size of 81 nm.[46] Typically, PXRD only determines the crystalline size and not the particle size; however, in the case of nanosized particle, the crystallite and particle size tend to be the same. As a second method, the TEM data show that the particles are ∼80 ± 10 nm in size. Both of these measurements account for the fact that the SSHT method is suitable for the production of nanoparticles in a nonaggregated form.

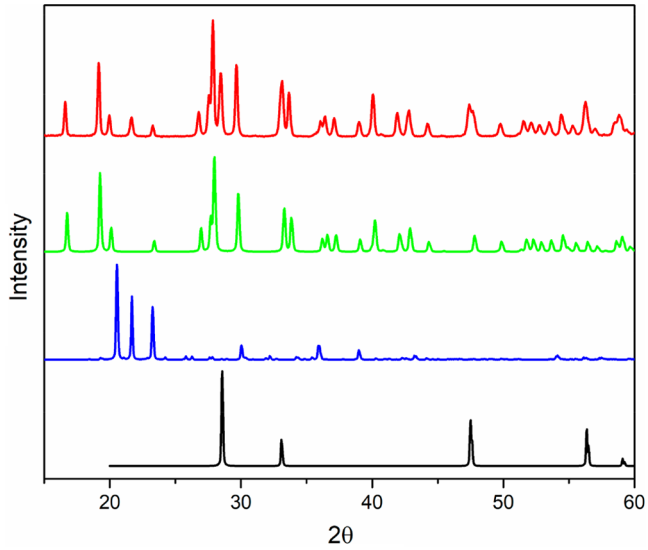

Figure 4. Powder X-ray diffraction patterns of standards CeO_2 (black) (04-003-2611), SiO_2 (blue) (04-016-2556), $Lu_2Si_2O_7$ (green) (04-010-9417), and the experimental scintillating $Lu_2Si_2O_7$:Ce^{3+} nanoparticles by SSHT at 1000 °C (red).

The zeta-potential values (Figure S1) for the Stober silica nanoparticles become negative and increase as the pH of the solution increases because of the deprotonation of the surface hydroxyl groups at this pH, which accounts for the stability of the nanoparticles in aqueous media. After calcination the surface charge remain largely negative as expected and indicates that even after the SSHT treatment not all surface hydroxyl groups were removed. This can be useful in the functionalization of these particles for future biomedical applications such as optogenetics.[47,48]

Figure 4 shows the powder X-ray diffraction (PXRD) patterns of the nanoparticles prepared using the SSHT method, and for comparison, Figure 5 shows the PXRD patterns of the nanoparticles heated at 1200 °C without the use of a salt support and of the sample prepared by solid state method at 1400 °C. As can be seen from Figure 4, the nanoparticles synthesized using the SSHT method at 1000 °C, the characteristic diffraction patterns confirm the presence of the $Lu_2Si_2O_7$ phase and indicate the presence of only minimal amounts of CeO_2 and unreacted silica. The important result is that the product nanoparticle consists of a single silicate phase, $Lu_2Si_2O_7$. By comparison, when the nanoparticles were calcined at 1200 °C, without the use of a salt support at significantly higher temperatures than the SSHT method, complete phase formation occurs in only 15 min. However, the product nanoparticles consist of a mixture of cerium-doped $Lu_2Si_2O_7$ and Lu_2SiO_5. These results are illustrated in Figure 5. Clearly, the ability of the SSHT method to allow heating the samples for longer times at lower temperature enables the selective synthesis of only a single silica phase nanoparticle product. For the sample prepared by solid state method at 1400 °C, the particles consisted of two phases: $Lu_2Si_2O_7$ and Lu_2SiO_5. Based on XRD peak broadening, the powder had crystallite sizes of 360 nm.[49]

DOI: 10.1021/acsanm.8b02146
ACS Appl. Nano Mater. 2019, 2, 1857−1865

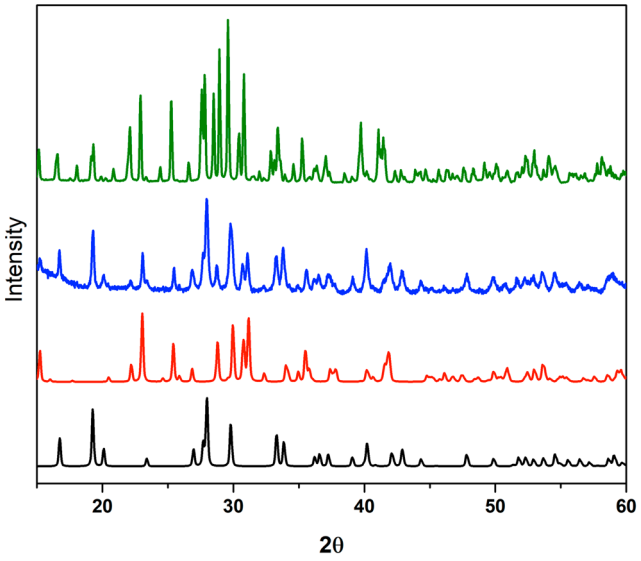

Figure 5. Powder X-ray diffraction pattern of standards $Lu_2Si_2O_7$ (black) (04-010-9417), Lu_2SiO_5 (red) (04-013-1146), and the experimental scintillating lutetium silicate:Ce^{3+} nanoparticles calcined at 1200 °C (blue) and the experimental scintillating Lutetium silicate:Ce^{3+} sample prepared by solid state method at 1400 °C (green).

The luminescence of all nanoparticles was checked by irradiating them with 365 nm UV light. Samples that displayed luminescence were checked for scintillation using the Cu X-rays of the powder diffractometer. As can be seen from Figure 6, these nanoparticles both scintillated and luminesced in a bright blue color. Sintered particles synthesized by the traditional solid state technique were also checked for luminescence and scintillation. Figure 7 illustrates the observed bright blue luminescence and scintillation.

Quantitative luminescence data for nanoparticles as well as for a sample prepared by solid state synthesis were obtained on a PerkinElmer S55 fluorometer as shown in Figure 8. The commercial sample by phosphor technology required the use of a 1% attenuator after a 10 times dilution with pure KBr to decrease the intensity of the signal to a measurable level. This data is shown in Figure S4. The sample synthesized by the solid state route required the use of a 10% attenuator to decrease the intensity of the signal to measurable levels. The fluorescence emission spectrum featured a large peak at 358 nm. The intensity as well as the visual luminescence was more intense in the sample prepared by solid state compared to the nanoparticle sample. It is likely that the samples prepared via the solid state synthesis at 1400 °C contain lower amounts of surface hydroxyl groups, which helps to decrease a non-radiative relaxation process.[50] Nanoparticles usually have a higher surface area, which gives rise to larger amounts of unsaturated and dangling bonds in these particles as well as a high level of surface hydroxyl groups.[51] This is the likely reason for the lower luminescence intensity of the nanoparticle phase compared to the sample prepared by the solid state synthesis method. The photoluminescence excitation spectra of the solid state powder as well as the $Lu_2Si_2O_7$ sample shows an asymmetric broad peak around ~400 nm, which corresponds to the electron transitions from 4f ground state to a 5d transition state of Ce^{3+}. The scintillation mechanism consists of primary and secondary processes. The primary process is the transfer of energy from ionizing radiation (X-ray) to the Ce^{3+} luminescent centers.[52] Literature precedent suggests that in the lattice of the $Lu_2Si_2O_7$:Ce^{3+} phase the Ce^{3+} ions only substitutes for one crystallographic site.[27] The larger Ce centers which substitute for the smaller Lu sites act as the luminescence centers. The secondary process is by which the electron transitions from the lowest 5d level ($5d_1$) to the two sublevels of spin−orbit split of Ce^{3+}−$^2F_{5/2}$ and $^2F_{7/2}$ gives rise to the asymmetry on the photoluminescence spectra as seen in Figure 8.[27,53] The energy level diagram for this phenomenon is depicted in Figure S5. This asymmetry as well as the shoulder peak is more prominent in the radioluminescence spectra as shown in Figure 9 for the $Lu_2Si_2O_7$:Ce^{3+} SSHT nanoparticle system. The radioluminescence of the $Lu_2Si_2O_7$:Ce^{3+} SSHT nanoparticle system is red-shifted 117 nm compared to the photoluminescence spectra and the commercial powder from phosphor technology red-shifted 129 nm compared to the photoluminescence spectra. This could be because of the internal absorption of the host system of the nanoparticles.[53,54] The quantum yield of these nanoparticles is 20 ± 9%. Structural defects and dangling OH^- bonds act as and limit the quantum yield of the nanoparticles. This is comparable to and even better than some other luminescent nanoparticles.[55−57]

FTIR spectra for the as synthesized as well as for the calcined nanoparticles are shown in Figure 10. As is typical in the formation of nanoparticles, a large peaks around ~1100 and 1200 cm^{-1} can be attributed to Si−OH and Si−O−Si vibrations, respectively. The two bands at ~760 and ~850 cm^{-1} are ascribed to the symmetric and asymmetric vibrations of the Si−O bonds. The band at around ~900 cm^{-1} corresponds to the free $Si-O^-$ moieties.[58]

The SSHT method enables the synthesis of single phase scintillating nanoparticles but does add an additional processing step. The water-soluble Cs_2SO_4 needs to be removed, and the nanoparticles need to be isolated. This requires repeated washings to ensure that the Cs_2SO_4 is fully removed from the nanoparticle surface. To achieve complete removal of Cs_2SO_4, as it is toxic to cells and therefore not appropriate for biomedical application, the Cs^+ ions that remained electrostatically attached to the surface were removed by an ion exchange step using a dilute acid (1 M

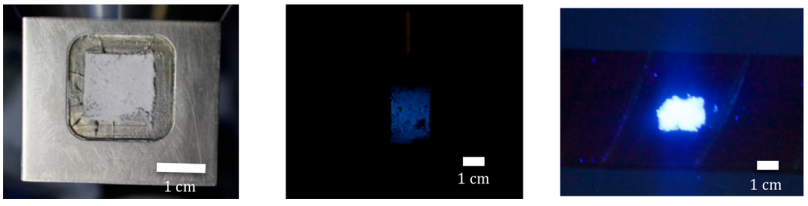

Figure 6. $Lu_2Si_2O_7$:Ce^{3+} nanoparticle sample prepared using the SSHT method calcined at 1000 °C under visible (left) and X-ray irradiation (Cu Kα, wavelength 1.5405 Å) (middle) and UV irradiation (right).

DOI: 10.1021/acsanm.8b02146
ACS Appl. Nano Mater. 2019, 2, 1857−1865

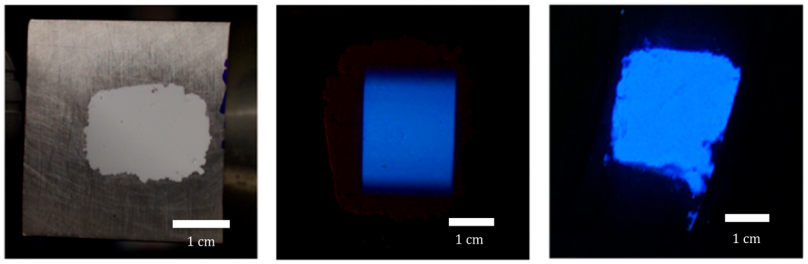

Figure 7. Sample prepared by solid state method at 1400 °C under visible (left) and X-ray irradiation (Cu Kα, wavelength 1.5418 Å (middle) and UV irradiation (right)

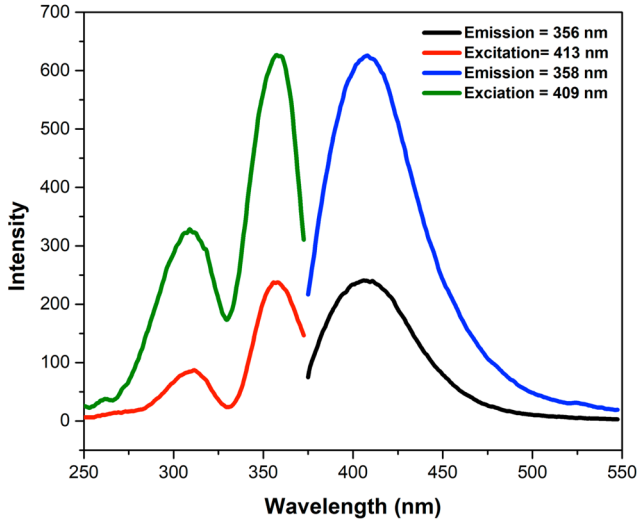

Figure 8. Photoluminescence spectra (black and blue) and photoluminescence excitation (red and green) spectra of lutetium silicate:Ce^{3+} sample prepared by solid state reaction at 1400 °C (red and black) and the $Lu_2Si_2O_7$:Ce^{3+} nanoparticles prepared by the SSHT method and calcined at 1000 °C (blue and green).

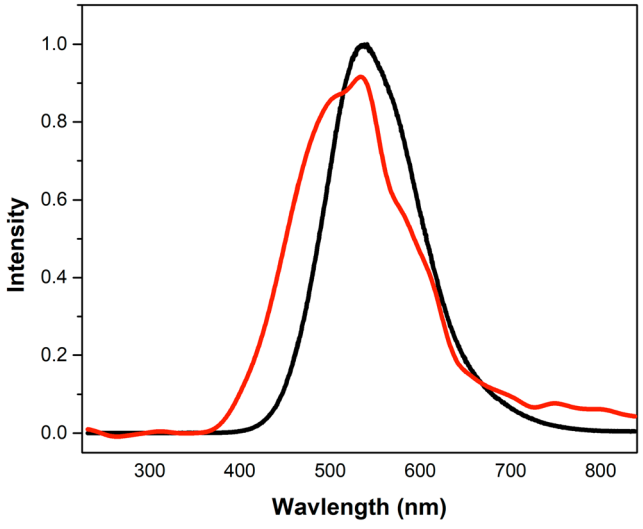

Figure 9. Radioluminescence spectra of $Y_2Si_2O_7$:Ce^{3+} commercial powder by phosphor technology (black) and $Lu_2Si_2O_7$:Ce^{3+} nanoparticles prepared by the SSHT method and calcined at 1000 °C (red).

HCl) or dilute salt solution (1 M NaCl). TEM images revealed (Figures 2D and 2E, respectively) that when the nanoparticles were treated with 1 M HCl or saturated NaCl, they did not

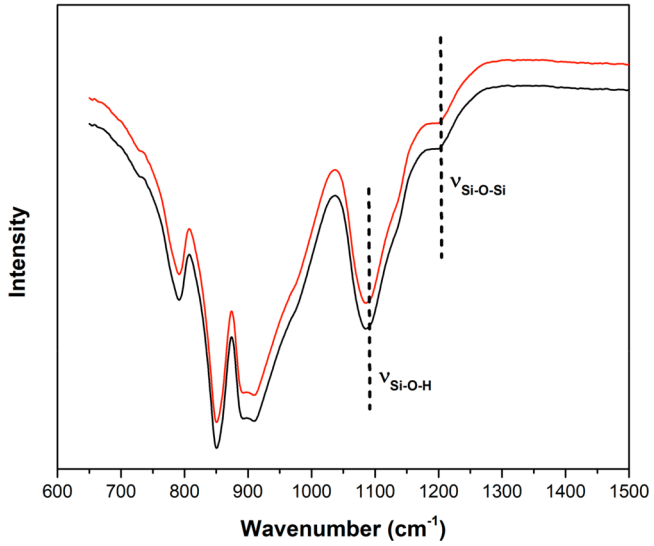

Figure 10. FTIR spectra of as synthesized $Lu_2Si_2O_7$:Ce^{3+} nanoparticles (black) and calcined nanoparticles (red).

retain their morphology. However, ion exchange using a 1 M NaCl solution left the nanoparticles unchanged; they retained their morphology and their scintillation and luminescing abilities. This can be seen very clearly in the TEM image in Figure 2F. EDS still detects a small amount of cesium on the surface, and consequently, future studies are planned to develop a simple technique to remove all the cesium from the surface of the nanoparticles.

CONCLUSIONS

This study details a new methodology that utilizes a facile core−shell approach combined with the salt-supported high temperature method (SSHT) to prepare compositions that would otherwise be difficult to synthesize on the nanoscale. These findings show that the key to obtaining isolated nanoparticles of the lutetium orthosilicate phase is to utilize a salt support, such as Cs_2SO_4, that functions to spatially isolate the nanoparticles, thereby preventing them from aggregating when heated to 1000 °C for 48 h. This SSHT method allows for longer calcination times at high temperatures without the issue of particle aggregation or necking and, moreover, gives rise to the formation of single phase $Lu_2Si_2O_7$ nanoparticles that could not otherwise be obtained by calcining at higher temperatures for brief time periods.

Nanoparticles could be readily isolated by dissolving and thus removing the Cs_2SO_4 and by exchanging any remaining Cs^+ ions electrostatically bonded to the surface by using 1 M NaCl. These nanoparticles display very strong luminescence

DOI: 10.1021/acsanm.8b02146
ACS Appl. Nano Mater. 2019, 2, 1857−1865

and scintillation abilities. Coupled with their size, 100 nm, these nanoparticles could be suitable for biomedical applications. The chemical insights discussed in this study can be used to guide the development of other scintillating nanoparticles as well as the synthesis of other ternary or quaternary phases at the nanoscale. This "solid state chemistry at the nanoscale" opens up a whole new synthetic approach for preparing complex phases as nanoparticles.

EXPERIMENTAL SECTION

Materials. Tetraethyl orthosilicate (TEOS, Fisher Scientific, 99+ %), ammonium hydroxide (VWR, 28−30%), cerium nitrate (Reacton, 99.99%), lutetium nitrate (Fisher Scientific, 99.9%), urea (Fisher Scientific, 100%), methanol (99.9%, Sigma-Aldrich), deionized double distilled water (ACS reagent grade), cesium sulfate (Fisher Scientific, 99.99%), sodium chloride (Fisher Scientific, 99.99%), hydrochloric acid (Fisher Scientific, 99.99%), Lu_2O_3 (Fisher Scientific, 99.999%), SiO_2 (Fisher Scientific, 99.999%), and CeO_2 (Fisher Scientific, 99.999%) were utilized in this study. CeO_2, SiO_2, and cesium sulfate were prefired at 260 °C. Lu_2O_3 was prefired at 1000 °C.

Synthesis of Stober Silica Nanoparticles. Stober silica nanoparticles were synthesized following the methods found in the literature.[43] In brief, water (13.85 mL) and ammonium hydroxide (23.65 mL), 28% by weight, were added to a round-bottom flask, and the mixture was heated at 60 °C, at which point tetraethyl orthosilicate (TEOS) (3.80 mL) was added. To allow for the hydrolysis and the polycondensation of the silicon source, the mixture was aged for 2 h. The nanoparticles were isolated by centrifugation at 8000 rpm. The nanoparticles were washed and centrifuged 4−5 times until the ammonia had been removed from the system and the pH of the water remained unchanged. The isolated nanoparticles were dried at 90 °C overnight, and their size and uniformity were checked by TEM.

Coating of Nanoparticles with Cerium and Lutetium; Formation of the Orthosilicate Phase. The nanoparticles were sequentially coated with cerium and lutetium by using a dilute coating procedure. $Ce(NO_3)_3$ (0.1 g) and urea (0.0674 g) were added to the Stober silica particles (50 mg) in water (50 mL), sonicated to ensure homogeneity, and stirred at 90 °C for 6 h.[10,42] The particles were isolated via centrifugation, washed with water, and dried at 90 °C overnight. The dry particles were redispersed in water (3.33 mg/mL), sonicated, and coated with $Lu(NO_3)_3$ (0.4 g) and urea (0.0337 g) using the same procedure and isolated via centrifugation. To react the SiO_2, Lu_2O_3, and Ce^{3+} to create the scintillating crystalline phase, these particles were ground with 100 times their weight of Cs_2SO_4. The mixture was placed inside a silica tube that was evacuated and sealed. The tube was heated for 2 days at 1000 °C to obtain the desired phase, as determined by powder X-ray diffraction. The $Lu_2Si_2O_7$:Ce nanoparticles were sonicated and washed with water to dissolve the Cs_2SO_4 and isolated via centrifugation. The process was repeated twice to ensure that all of the Cs_2SO_4 is removed. In the final step, the nanoparticles were washed with 1 M NaCl/1 M HCl to ensure that any surface adsorbed Cs is exchanged with the Na^+/ H^+ and removed.

Powder X-ray Diffraction (PXRD). PXRD patterns were collected on a Rigaku Ultima IV diffractometer using Cu Kα radiation (λ = 1.5418 Å) and a D/Tex high-speed detector. Patterns were collected in the angular range of 5°−65° 2θ with a step size of 0.02°.

Optical Properties. Fluorescence data were collected on ground samples of $Lu_2Si_2O_7$:Ce nanoparticles using a PerkinElmer LS55 luminescence spectrometer. Excitation spectra were collected at emission wavelengths of 358−356 nm, and emission scans were collected at excitation wavelengths of 409−413 nm for the nanoparticle sample prepared by SSHT and solid state methods.

Radioluminescence (RL) was measured with a Amptek Mini-X Ag source at 40 kV and 99 μA, a Horiba JY Synapse CCD camera, and a Horiba JY microHR monochromator with a grating of 300 grooves/mm, a blaze of 600 nm, and a slit width of 1 mm. Light was collected from a 600 m Ocean Optics fiber. The integration time was adjusted to 1 s. Samples were packed in a 3D printed 10 mm × 1 mm round washer made from clear ploy lactic acid lament. All optical properties were compared to commercial YSO:Ce and performed at ambient conditions. Quantum yield measurements were acquired on an Edinburgh FS5 fluorescence spectrometer equipped with a 150 W continuous wave xenon lamp source for excitation.

Scintillation images of $Lu_2Si_2O_7$Ce nanoparticles were obtained using a digital camera placed inside a Rigaku Ultima IV diffractometer equipped with a Cu Kα source (λ = 1.54056 Å). As a qualitative indicator of intensity, a scintillation image of $LuSiO_5$:Ce^{3+} (0.5 atom % Ce in Lu) was also taken. This sample was prepared via the solid state reaction of Lu_2O_3, CeO_2, and SiO_2 and heated at 1400 °C for a total of 6 days with intermittent grindings every 2 days.

Infrared spectroscopy was performed using a PerkinElmer spectrum 100 FT-IR spectrometer with a diamond ATR attachment. IR spectra were recorded in the spectral range of 4000 to 650 cm^{-1}. Final IR spectra consist of 32 total averaged scans.

Energy-Dispersive Spectroscopy (EDS). EDS was performed on a nanoparticle product using a Tescan Vega-3 SEM equipped with a Thermo EDS attachment. The SEM was operated in low-vacuum mode. The powders were mounted on an SEM stub with carbon tape and analyzed using a 20 kV accelerating voltage and an 80 s accumulating time.

Transmission Electron Microscopy (TEM). TEM measurements were performed on a Hitachi H-7800 TEM and analyzed using a 120 kV accelerating voltage at various magnifications. To prepare samples for the TEM, nanoparticle samples were diluted in ethanol and sonicated for 15 min to ensure homogeneity. A drop of dilute sample suspended in ethanol was placed on a copper grid with a thin Formvar polymer coating and completely dried at room temperature prior to the measurement.

Zeta-Potential Measurements. These measurements were conducted on samples in the appropriate pH solutions (pH 2−6). The samples were prepared by placing a small amount of sample into a disposable plastic centrifuge tube and sonicating the tube for 5 min (1510 Sonicator, Branson). The suspension was then tested for zeta potential using a Zetazizer nanoZS (Malvern).

ASSOCIATED CONTENT

Supporting Information

The Supporting Information is available free of charge on the ACS Publications website at DOI: 10.1021/acsanm.8b02146.

Figures S1−S5 and Table S1 (PDF)

AUTHOR INFORMATION

Corresponding Author

*E-mail: zurloye@mailbox.sc.edu.

ORCID

Shani Egodawatte: 0000-0001-8551-8885

Stephen H. Foulger: 0000-0002-4221-2154

Hans-Conrad zur Loye: 0000-0001-7351-9098

Notes

The authors declare no competing financial interest.

ACKNOWLEDGMENTS

This work was supported by the National Science Foundation Grant OIA-1032881. T.J.P. and G.R.G. were supported in part by the South Carolina Honors College Exploration Scholars Research Program. John Estock and Houston Bennet are gratefully acknowledged for help at the start of the project.

REFERENCES

(1) Endo, T.; Yoshimura, T.; Esumi, K. Synthesis and Catalytic Activity of Gold−Silver Binary Nanoparticles Stabilized by PAMAM Dendrimer. *J. Colloid Interface Sci.* **2005**, *286*, 602−609.

DOI: 10.1021/acsanm.8b02146
ACS Appl. Nano Mater. 2019, 2, 1857−1865

(2) Coowanitwong, N.; Wu, C.-Y.; Cai, M.; Ruthkosky, M.; Rogers, J.; Feng, L.; Watano, S.; Yoshida, T. Surface Modification of Al_2O_3 Fiber with Binary Nanoparticles using a Dry-Mechanical Coating Technique. *J. Nanopart. Res.* **2003**, *5*, 247−258.
(3) Bilecka, I.; Djerdj, I.; Niederberger, M. One-Minute Synthesis of Crystalline Binary and Ternary Metal Oxide Nanoparticles. *Chem. Commun.* **2008**, No. 7, 886−888.
(4) Rogach, A. L.; Kornowski, A.; Gao, M.; Eychmüller, A.; Weller, H. Synthesis and Characterization of a Size Series of Extremely Small ThiolSstabilized CdSe Nanocrystals. *J. Phys. Chem. B* **1999**, *103*, 3065−3069.
(5) Loitongbam, R. S.; Singh, W. R.; Phaomei, G.; Singh, N. S. Blue and Green Emission from Ce^{3+} and Tb^{3+} Co-doped Y_2O_3 Nanoparticles. *J. Lumin.* **2013**, *140*, 95−102.
(6) Green, M.; Harwood, H.; Barrowman, C.; Rahman, P.; Eggeman, A.; Festry, F.; Dobson, P.; Ng, T. A Facile Route to CdTe Nanoparticles and Their Use in Bio-Labelling. *J. Mater. Chem.* **2007**, *17*, 1989−1994.
(7) Rogach, A. L. Nanocrystalline CdTe and CdTe (S) Particles: Wet Chemical Preparation, Size-Dependent Optical Properties and Perspectives of Optoelectronic Applications. *Mater. Sci. Eng., B* **2000**, *69*, 435−440.
(8) Ma, W.; Luther, J. M.; Zheng, H.; Wu, Y.; Alivisatos, A. P. Photovoltaic Devices Employing Ternary PbS_xSe_{1-x} Nanocrystals. *Nano Lett.* **2009**, *9*, 1699−1703.
(9) Shi, W.; Zeng, H.; Sahoo, Y.; Ohulchanskyy, T. Y.; Ding, Y.; Wang, Z. L.; Swihart, M.; Prasad, P. N. A General Approach to Binary and Ternary Hybrid Nanocrystals. *Nano Lett.* **2006**, *6*, 875−881.
(10) Fan, L.; Lin, D.; Zhang, X.; Shi, Y.; Zhang, J.; Xie, J.; Lei, F.; Zhang, L. Local Structures of Lu Atoms in a Core−Shell Approach for Synthesis of Lu_2SiO_5 phase. *Chem. Phys. Lett.* **2016**, *644*, 41−44.
(11) Li, D.; Egodawatte, S.; Kaplan, D. I.; Larsen, S. C.; Serkiz, S. M.; Seaman, J. C.; Scheckel, K. G.; Lin, J.; Pan, Y. Sequestration of U(VI) from Acidic, Alkaline, and High Ionic-Strength Aqueous Media by Functionalized Magnetic Mesoporous Silica Nanoparticles: Capacity and Binding Mechanisms. *Environ. Sci. Technol.* **2017**, *51*, 14330−14341.
(12) Tsuzuki, T.; McCormick, P. G. Mechanochemical Synthesis of Nanoparticles. *J. Mater. Sci.* **2004**, *39*, 5143−5146.
(13) Mao, R.; Zhang, L.; Zhu, R.-Y. Optical and Scintillation Properties of Inorganic Scintillators in High Energy Physics. *IEEE Trans. Nucl. Sci.* **2008**, *55*, 2425−2431.
(14) Zhao, W.; Ristic, G.; Rowlands, J. X-ray Imaging Performance of Structured Cesium Iodide Scintillators. *Med. Phys.* **2004**, *31*, 2594−2605.
(15) Lempicki, A.; Brecher, C.; Szupryczynski, P.; Lingertat, H.; Nagarkar, V.; Tipnis, S.; Miller, S. A New Lutetia-Based Ceramic Scintillator for X-ray Imaging. *Nucl. Instrum. Methods Phys. Res., Sect. A* **2002**, *488*, 579−590.
(16) Nassalski, A.; Kapusta, M.; Batsch, T.; Wolski, D.; Mockel, D.; Enghardt, W.; Moszynski, M. Comparative Study of Scintillators for PET/CT Detectors. *IEEE Nuclear Science Symposium Conference Record, 2005, IEEE* **2005**, 2823−2829.
(17) Fernández-Carrión, A. J.; Allix, M.; Ocaña, M.; García-Sevillano, J.; Cusso, F.; Fitch, A. N.; Suard, E.; Becerro, A. I. Crystal Structures and Photoluminescence Across the $La_2Si_2O_7$−$Ho_2Si_2O_7$ System. *Inorg. Chem.* **2013**, *52*, 13469−13479.
(18) Gerdes, R.; Bettentrup, H.; Enseling, D.; Haase, M.; Jüstel, T. On the Synthesis, Phase Optimisation and Luminescence of Some Rare Earth Pyrosilicates. *J. Lumin.* **2017**, *190*, 451.
(19) Horiai, T.; Kurosawa, S.; Murakami, R.; Yamaji, A.; Shoji, Y.; Ohashi, Y.; Pejchal, J.; Kamada, K.; Yokota, Y.; Yoshikawa, A. Crystal Growth and Optical Properties of Gd Admixed Ce-doped $Lu_2Si_2O_7$ Single Crystals. *J. Cryst. Growth* **2017**, *468*, 391−394.
(20) Yan, C.; Zhao, G.; Hang, Y.; Zhang, L.; Xu, J. Czochralski Growth and Crystal Structure of Cerium-Doped $Lu_2Si_2O_7$ Scintillator. *Mater. Lett.* **2006**, *60*, 1960−1963.
(21) Lecoq, P. Development of New Scintillators for Medical Applications. *Nucl. Instrum. Methods Phys. Res., Sect. A* **2016**, *809*, 130−139.
(22) Ren, G.; Qin, L.; Lu, S.; Li, H. Scintillation Characteristics of Lutetium Oxyorthosilicate (Lu_2SiO_5: Ce) Crystals Doped with Cerium Ions. *Nucl. Instrum. Methods Phys. Res., Sect. A* **2004**, *531*, 560−565.
(23) Gervais, M.; Le Floch, S.; Rifflet, J. C.; Coutures, J.; Coutures, J. P. Effect of the Melt Temperature on the Solidification Process of Liquid Garnets $Ln_3Al_5O_{12}$ (Ln= Dy, Y, and Lu). *J. Am. Ceram. Soc.* **1992**, *75*, 3166−3168.
(24) Do Han, S.; Khatkar, S.; Taxak, V.; Kumar, D.; Park, J.-Y. Combustion Synthesis and Luminescent Properties of Eu^{3+}-Doped $LnAlO_3$ (Ln= Y and Gd) phosphors. *Mater. Sci. Eng., B* **2006**, *127*, 272−275.
(25) Sokolnicki, J. Upconversion Luminescence from Er^{3+} in Nanocrystalline $Y_2Si_2O_7$: Er^{3+} and $Y_2Si_2O_7$: Yb^{3+}, Er^{3+} phosphors. *Mater. Chem. Phys.* **2011**, *131*, 306−312.
(26) Marciniak, L.; Hreniak, D.; Dobrowolska, A.; Zych, E. Size-dependent luminescence in $Y_2Si_2O_7$ nanoparticles doped with Ce^{3+} ions. *Appl. Phys. A: Mater. Sci. Process.* **2010**, *99*, 871−877.
(27) Jary, V.; Nikl, M.; Kurosawa, S.; Shoji, Y.; Mihokova, E.; Beitlerova, A.; Pazzi, G. P.; Yoshikawa, A. Luminescence Characteristics of the Ce^{3+}-Doped Pyrosilicates: The Case of La-admixed $Gd_2Si_2O_7$ single crystals. *J. Phys. Chem. C* **2014**, *118*, 26521−26529.
(28) Fernández-Carrión, A. J.; Ocaña, M.; Florian, P.; García-Sevillano, J.; Cantelar, E.; Fitch, A. N.; Suchomel, M. R.; Becerro, A. I. Crystal Structure and Luminescent Properties of Eu^{3+}-Doped A-$La_2Si_2O_7$ tetragonal phase stabilized by spray pyrolysis synthesis. *J. Phys. Chem. C* **2013**, *117*, 20876−20886.
(29) Wei, Q.; Liu, G.; Zhou, Z.; Wan, J.; Yang, H.; Liu, Q. Preparation and Spectroscopic Properties of Ce-Doped $La_2Si_2O_7$ as Novel Scintillator Materials. *Mater. Lett.* **2014**, *126*, 178−180.
(30) Bohem, M. E.; Pook, N.-P.; Adam, A.; Tran, T. T.; Halasyamani, P. S.; Entenmann, M.; Schleid, T. Luminescence and Scintillation Properties of $La_2[Si_2O_7]$: Ce^{3+} Functional Pigment−A Concept for UV-Protection of Coatings. *Dyes Pigm.* **2015**, *123*, 331−340.
(31) Zhang, Z.; Wang, Y.; Zhang, F.; Cao, H. Electronic Structures and Eu^{3+} Photoluminescence Behaviors in $Y_2Si_2O_7$ and $La_2Si_2O_7$. *J. Alloys Compd.* **2011**, *509*, 5023−5027.
(32) Fernández-Carrión, A. J.; Ocaña, M.; García-Sevillano, J.; Cantelar, E.; Becerro, A. I. New Single-Phase, White-Light-Emitting Phosphors Based on δ-$Gd_2Si_2O_7$ for Solid-State Lighting. *J. Phys. Chem. C* **2014**, *118*, 18035−18043.
(33) Tang, X.; Gao, Y.; Chen, H.; Luo, H. Hydrothermal Synthesis of Lutetium Disilicate Nanoparticles. *J. Solid State Chem.* **2012**, *188*, 38−43.
(34) Ohashi, H.; Alba, M.; Becerro, A.; Chain, P.; Escudero, A. Structural Study of the $Lu_2Si_2O_7$−$Sc_2Si_2O_7$ System. *J. Phys. Chem. Solids* **2007**, *68*, 464−469.
(35) Liu, P.; Lv, S.; Chen, X.; Tang, J.; Li, J.; Zhou, S. Crystallization Control Toward Colorless Cerium-Doped Scintillating Glass. *Opt. Express* **2018**, *26*, 20582−20589.
(36) Lv, S.; Cao, M.; Li, C.; Li, J.; Qiu, J.; Zhou, S. In-Situ Phase Transition Control in the Supercooled State for Robust Active Glass Fiber. *ACS Appl. Mater. Interfaces* **2017**, *9*, 20664−20670.
(37) Burzo, E. *Sorosilicates*; Springer: Berlin, 2005; pp 1−28.
(38) Huang, X.; El-Sayed, M. A. Gold nanoparticles: Optical Properties and Implementations in Cancer Diagnosis and Photothermal Therapy. *Journal of Advanced Research* **2010**, *1*, 13−28.
(39) Gupta, A. K.; Gupta, M. Synthesis and Surface Engineering of Iron Oxide Nanoparticles for Biomedical Applications. *Biomaterials* **2005**, *26*, 3995−4021.
(40) Dykman, L.; Khlebtsov, N. Gold Nanoparticles in Biomedical Applications: Recent Advances and Perspectives. *Chem. Soc. Rev.* **2012**, *41*, 2256−2282.
(41) Egodawatte, S.; Dominguez, S.; Larsen, S. C. Solvent Effects in the Development of a Drug Delivery System for 5-Fluorouracil Using

DOI: 10.1021/acsanm.8b02146
ACS Appl. Nano Mater. 2019, 2, 1857−1865

Magnetic MesoporousSsilica Nanoparticles. *Microporous Mesoporous Mater.* **2017**, *237*, 108−116.
(42) Yermolayeva, Y. V.; Korshikova, T. I.; Tolmachev, A. V.; Yavetskiy, R. P. X-ray Luminescence of Core-Shell Structured SiO_2/Lu_2O_3:Eu^{3+} and SiO_2/Lu2Si2O7:Eu^{3+} particles. *Radiat. Meas.* **2011**, *46*, 551−554.
(43) Nozawa, K.; Gailhanou, H.; Raison, L.; Panizza, P.; Ushiki, H.; Sellier, E.; Delville, J.; Delville, M. Smart Control of Monodisperse Stöber Silica Particles: Effect of Reactant Addition Rate on Growth Process. *Langmuir* **2005**, *21*, 1516−1523.
(44) Gordon, W. O.; Carter, J. A.; Tissue, B. M. Long-Lifetime Luminescence of Lanthanide-Doped Gadolinium Oxide Nanoparticles for Immunoassays. *J. Lumin.* **2004**, *108*, 339−342.
(45) Nagpure, I. M.; Shinde, K. N.; Kumar, V.; Ntwaeaborwa, O. M.; Dhoble, S. J.; Swart, H. C. Combustion Synthesis and Luminescence Investigation of $Na_3Al_2(PO_4)_3$:RE (RE = Ce^{3+}, Eu^{3+} and Mn^{2+}) Phosphor. *J. Alloys Compd.* **2010**, *492*, 384−388.
(46) Patterson, A. The Scherrer Formula for X-ray Particle Size Determination. *Phys. Rev.* **1939**, *56*, 978.
(47) Jenkins, R.; Bandera, Y. P.; Daniele, M. A.; Ledford, L. L.; Tietje, A.; Kelso, A. A.; Sehorn, M. G.; Wei, Y.; Chakrabarti, M.; Ray, S. K.; Foulger, S. H. Sequestering Survivin to Functionalized Nanoparticles: A Strategy to Enhance Apoptosis in Cancer Cells. *Biomater. Sci.* **2016**, *4*, 614−626.
(48) Jetty, R.; Bandera, Y. P.; Daniele, M. A.; Hanor, D.; Hung, H.-I.; Ramshesh, V.; Duperreault, M. F.; Nieminen, A.-L.; Lemasters, J. J.; Foulger, S. H. Protein Triggered Fluorescence Switching of Near-Infrared Emitting Nanoparticles for Contrast-Enhanced Imaging. *J. Mater. Chem. B* **2013**, *1*, 4542−4554.
(49) Becerro, A.; Escudero, A. Polymorphism in the $Lu_{2-x}Y_xSi_2O_7$ System at High Temperatures. *J. Eur. Ceram. Soc.* **2006**, *26*, 2293−2299.
(50) Patra, A. Effect of Crystal Structure and Concentration on Luminescence in Er^{3+}:ZrO_2 nanocrystals. *Chem. Phys. Lett.* **2004**, *387*, 35−39.
(51) Wang, S.-F.; Sun, G.-Z.; Fang, L.-M.; Lei, L.; Xiang, X.; Zu, X.-T. A Comparative Study of $ZnAl_2O_4$ Nanoparticles Synthesized From Different Aluminum Salts for Use as Fluorescence Materials. *Sci. Rep.* **2015**, *5*, 12849.
(52) Suzuki, H.; Tombrello, T.; Melcher, C.; Schweitzer, J. Light Emission Mechanism of $Lu_2(SiO_4)$ O: Ce. *IEEE Trans. Nucl. Sci.* **1993**, *40*, 380−383.
(53) Wei, Q.; Zhuang, J.; Liu, G.; Zhou, Z.; Yang, H.; Wang, J.; Liu, Q. Preparation and Luminescence Properties of SiO_2/$Lu_2Si_2O_7$: Ce composite starting from mesopore template. *RSC Adv.* **2014**, *4*, 33819−33825.
(54) Wan, H.; Wang, Y.; Zhuang, L.; Huang, S.; Zhang, Z.; Xu, Z.; Mao, R.; Feng, H.; Zhao, J. Photoluminescence, Scintillation Properties and Trap States of $La_2Si_2O_7$:Ce single crystal. *Mater. Res. Express* **2018**, *5*, No. 086202.
(55) Dantelle, G. r.; Fleury, B.; Boilot, J.-P.; Gacoin, T. How to Prepare the Brightest Luminescent Coatings? *ACS Appl. Mater. Interfaces* **2013**, *5*, 11315−11320.
(56) Rogach, A. L.; Nagesha, D.; Ostrander, J. W.; Giersig, M.; Kotov, N. A. Raisin bun"-Type Composite Spheres of Silica and Semiconductor Nanocrystals. *Chem. Mater.* **2000**, *12*, 2676−2685.
(57) Das, B.; Hossain, M.; Pramanick, A.; Dey, A.; Ray, M. One-pot Synthesis of Gel Glass Embedded with Luminescent Silicon Nanoparticles. *ACS Appl. Mater. Interfaces* **2019**, *11*, 2507.
(58) Al-Oweini, R.; El-Rassy, H. Synthesis and Characterization by FTIR Spectroscopy of Silica Aerogels Prepared Using Several $Si(OR)_4$ and $R''Si(OR')_3$ Precursors. *J. Mol. Struct.* **2009**, *919*, 140−145.

DOI: 10.1021/acsanm.8b02146
ACS Appl. Nano Mater. 2019, 2, 1857−1865